PHYSICAL REVIEW D **92,** 114014 (2015)

Dilepton production spectrum above T_c with a lattice quark propagator

Taekwang Kim,[*] Masayuki Asakawa,[†] and Masakiyo Kitazawa[‡]

Department of Physics, Osaka University, Toyonaka, Osaka 560-0043, Japan

(Received 1 June 2015; published 9 December 2015)

The dilepton production rate from the deconfined medium is analyzed with the photon self-energies constructed from quark propagators obtained by lattice numerical simulation for two values of temperature, $T = 1.5T_c$ and $3T_c$, above the critical temperature T_c. The photon self-energy is calculated by the Schwinger-Dyson equation with the lattice quark propagtor and a vertex function determined so as to satisfy the Ward-Takahashi identity. The obtained dilepton production rate at zero momentum exhibits divergences reflecting van Hove singularity and is significantly enhanced around $\omega \simeq T$ compared with the rate obtained by the perturbative analysis.

DOI: 10.1103/PhysRevD.92.114014 PACS numbers: 11.10.Wx, 14.60.-z

I. INTRODUCTION

Ultrarelativistic heavy ion collisions are a unique method for producing the deconfined medium experimentally on the Earth [1,2]. Various observables are measured in the experiments [1] to reveal properties of the deconfined medium and a variety of phenomena which come into play during the time evolution of the hot medium. Among these observables, the dilepton production yield has a characteristic feature that the yield provides us direct signals from the primordial deconfined medium [3] because dileptons once produced in the hot medium do not interact with and pass through the medium owing to their colorless nature.

The dilepton yield observed experimentally consists of the sum of the dilepton production in each stage of the time evolution of the hot medium. The dilepton production in heavy ion collisions is roughly classified into three processes except for the final state hadronic decays. The first one is the hard process, in which dileptons are produced by scatterings of hard partons in the colliding nuclei. The second and third processes are thermal radiations from the deconfined medium and confined medium, respectively. The dileptons in the low invariant mass region are usually expected to be dominated by these thermal radiations, while dileptons from the hard process have relatively high transverse momenta and large invariant masses. Experimental results on the dilepton production yield are usually compared with the baseline, called the "cocktail," which is the production yield estimated from the observed hadron abundances and their branching ratios into a dilepton pair. If there is no dilepton production from the hot medium, the dilepton production yield should be consistent with the cocktail result.

At the Relativistic Heavy Ion Collider (RHIC) at Brookhaven National Laboratory, e^+e^- pair production yield is measured by two collaborations, STAR and PHENIX [4,5]. Both of these collaborations reported that the pair production yield measured in Au + Au collisions at $\sqrt{s_{NN}} = 200$ GeV has significant enhancements in the low invariant mass (m) region compared with the cocktail [4–6], although the discrepancy in the magnitude of the enhancement between the two experimental groups has not been settled yet. The result of the PHENIX Collaboration shows that the yield at $m \simeq 500$ MeV is about one order larger than the cocktail [4].

When one performs an estimate of the dilepton production yield, one first calculates the dilepton production *rate* per unit time and unit volume from a static medium. The dilepton production *yield* is then given by the spacetime integral of the rate from each volume element of the medium. The dilepton production rate of a static medium is proportional to the imaginary part of the virtual photon self-energy [7–9]. When the temperature (T) is asymptotically high, the photon self-energy can be calculated perturbatively. Using the hard thermal loop (HTL) resummed perturbation theory [10,11], the dilepton production rate was calculated in Ref. [12] for lepton pairs with zero total three-momentum, and the result was extended in Ref. [13] to nonzero momentum. It is, however, nontrivial whether or not such perturbative analyses well describe the production rate from the deconfined medium near the critical temperature T_c, which has turned out to be a strongly coupled system [1]. Moreover, it is known that the perturbative analyses in Refs. [12,13] are modified by proper inclusion of higher-order terms [14]. The analysis of higher-order terms, however, is complicated, and it is still under debate whether the scheme is valid for the whole kinetic region [14,15]. For the description of the dilepton production rate in the deconfined phase near T_c, therefore, it is desirable to evaluate the rate without resort to perturbative methods. In particular, the large enhancement observed at PHENIX [4] suggests a possibility that the dilepton production from the strongly coupled medium above T_c has a large enhancement compared with the perturbative results used in the previous analyses [16].

[*]kim@kern.phys.sci.osaka-u.ac.jp
[†]yuki@phys.sci.osaka-u.ac.jp
[‡]kitazawa@phys.sci.osaka-u.ac.jp

There are several attempts at nonperturbative analyses for the dilepton production rate with lattice QCD [17,18]. When one investigates the rate on the lattice, one must take an analytic continuation from the imaginary-time correlator computable on the lattice to the real-time photon self-energy. This procedure, however, is an ill-posed problem, since the information on the imaginary-time correlators for discrete imaginary-time points obtained on the lattice is insufficient to reconstruct the continuous real-time function by itself [19]. In Ref. [18], an *Ansatz* for the spectral function is introduced to avoid this problem. An alternative way is to use Bayesian analysis, such as the maximum entropy method [19]. The lattice correlator, however, is insensitive to the structure of the spectrum in the low-energy region [20]. The estimate of the low-energy spectrum on the lattice, therefore, is a difficult problem with the presently existing methodologies.

The exact nonperturbative photon self-energy can be calculated by the Schwinger-Dyson equation (SDE) if we have the full quark propagator and the photon-quark vertex function. Recently, an analysis of the nonperturbative quark propagator above T_c was performed on the lattice in the quenched approximation in Landau gauge [21–23]. In this series of analyses, the Euclidean quark correlator obtained on the lattice with various bare quark mass and momentum are analyzed with several *Ansätze*. It has been shown [21–23] that the two-pole *Ansatz* for the real-time propagator, which was employed motivated by the study of fermion propagator at nonzero temperature [24,25], can reproduce the quark correlator obtained on the lattice over a rather wide range of these parameters. It is, therefore, expected that the obtained quark propagator well grasps the gist of the nonperturbative nature of the quark propagator.

The purpose of the present study is to analyze the dilepton production rate using this quark propagator. We construct the SDE with the quark propagators obtained on the lattice in Ref. [23] and with the vertex function constructed so as to satisfy the Ward-Takahashi identity (WTI). Our formalism, therefore, fulfills the conservation law of electric current. In this analysis, we show that the obtained dilepton production rate exhibits an enhancement of one order or more compared with the one from the free quark gas. Compared with the perturbative result in Ref. [12], our result has a qualitatively similar behavior at the low-m region, while it exhibits an enhancement around $m \simeq T$ owing to the van Hove singularity. The effect of the vetex correction is also discussed in detail.

The outline of this paper is as follows. In the next section we introduce the SDE for the photon self-energy and its components, the lattice quark propagator and a vertex function satisfying the WTI. In Sec. III, we then solve the SDE and present the form of the dilepton production rate in our formalism. The rate without the vertex correction is also calculated in this section. We then present the numerical result in Sec. IV. The final section is devoted to a short summary.

II. SCHWINGER-DYSON EQUATION FOR PHOTON SELF-ENERGY

A. Schwinger-Dyson equation

As dileptons are emitted from the decays of virtual photons, the dilepton production rate from a medium per unit time and unit volume is related to the retarded self-energy $\Pi^R_{\mu\nu}(\omega, \boldsymbol{q})$ of the virtual photon as [7–9]

$$\frac{d\Gamma}{d\omega d^3q} = \frac{\alpha}{12\pi^4}\frac{1}{Q^2}\frac{1}{e^{\beta\omega}-1}\mathrm{Im}\Pi^{R,\mu}_{\mu}(\omega, \boldsymbol{q}) \tag{1}$$

at the leading order of the fine structure constant α with $Q^2 = \omega^2 - \boldsymbol{q}^2$ and the inverse temperature $\beta = 1/T$. With the SDE in the Matsubara formalism, the exact photon self-energy is given by the full quark propagator $S(P)$ and the full photon-quark vertex $\Gamma_\mu(P+Q, P)$ as

$$\Pi_{\mu\nu}(i\omega_m, \boldsymbol{q}) = -\sum_{\mathrm{f}} e_{\mathrm{f}}^2 T \sum_n \int \frac{d^3p}{(2\pi)^3} \times \mathrm{Tr_C}\mathrm{Tr_D}[S(P)\gamma_\mu S(P+Q)\Gamma_\nu(P+Q, P)], \tag{2}$$

where $\omega_m = 2\pi T m$ and $\nu_n = (2n+1)\pi T$, with integers m and n representing the Matsubara frequencies for bosons and fermions, respectively, $P_\mu = (i\nu_n, \boldsymbol{p})$ is the four-momentum of quarks, and e_{f} is the electric charge of a quark with an index "f" representing the quark flavor. The color, flavor, and Dirac indices of $S(P)$ are suppressed for notational simplicity. $\mathrm{Tr_C}$ and $\mathrm{Tr_D}$ denote the trace over color and Dirac indices, respectively. We note that since we take the Landau gauge in this calculation, off-diagonal elements in color space disappear. As a result, the trace over the color indices gives a factor of 3 in Eq. (2). Equation (2) is graphically shown in Fig. 1, in which the shaded circles represent the full propagator and vertex

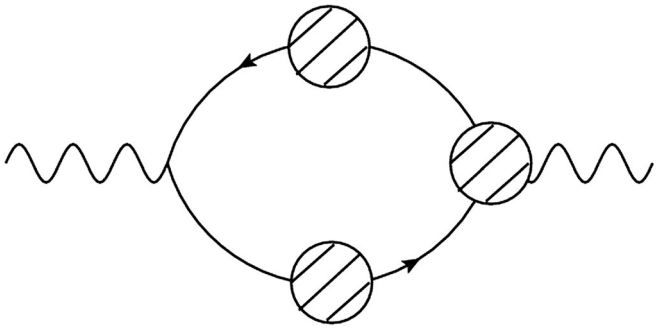

FIG. 1. Diagrammatic representation of the Schwinger-Dyson equation for the photon self-energy, Eq. (2). The shaded circles represent the full quark propagator and the full vertex function.

function. The retarded photon self-energy is obtained by the analytic continuation,

$$\Pi^R_{\mu\nu}(\omega,\boldsymbol{q}) = \Pi_{\mu\nu}(i\omega_m,\boldsymbol{q})|_{i\omega_m\to\omega+i\eta}. \tag{3}$$

In the following, we consider the two-flavor system with degenerate u and d quarks, in which $\sum_f e_f^2 = 5e^2/9$. In this study we also limit our attention to the $\boldsymbol{q}=0$ case.

B. Lattice quark propagator and spectral function

In the present study, we use the quark propagator obtained on the quenched lattice in Ref. [23] as the full quark propagator in Eq. (2). In this subsection, after a brief review on the general property of the quark propagator, we describe how to implement the results in Ref. [23] in our analysis.

On the lattice with a gauge fixing, one can measure the imaginary-time quark propagator,

$$S_{\mu\nu}(\tau,\boldsymbol{p}) = \int d^3x e^{-i\boldsymbol{p}\cdot\boldsymbol{x}}\langle\psi_\mu(\tau,\boldsymbol{x})\bar\psi_\nu(0,\boldsymbol{0})\rangle, \tag{4}$$

where $\psi_\mu(\tau,\boldsymbol{x})$ is the quark field with the Dirac index μ. Here, τ is the imaginary time restricted to the interval $0\le\tau<\beta$. For the moment, the Dirac indices μ and ν of the quark propagator are explicitly shown. The Fourier transform of the quark correlator,

$$S_{\mu\nu}(i\nu_n,\boldsymbol{p}) = \int_0^\beta d\tau e^{i\nu_n\tau}S_{\mu\nu}(\tau,\boldsymbol{p}), \tag{5}$$

is written in the spectral representation as

$$S_{\mu\nu}(i\nu_n,\boldsymbol{p}) = -\int_{-\infty}^{\infty}d\nu'\frac{\rho_{\mu\nu}(\nu',\boldsymbol{p})}{\nu'-i\nu_n} \tag{6}$$

with the quark spectral function $\rho_{\mu\nu}(\nu',\boldsymbol{p})$. The spectral function is related to the imaginary-time correlator Eq. (4) as

$$S_{\mu\nu}(\tau,\boldsymbol{p}) = \int_{-\infty}^{\infty}d\nu\frac{e^{(1/2-\tau/\beta)\beta\nu}}{e^{\beta\nu/2}+e^{-\beta\nu/2}}\rho_{\mu\nu}(\nu,\boldsymbol{p}). \tag{7}$$

In the deconfined phase in which the chiral symmetry is restored, the quark propagator anticommutes with γ_5. In this case, the spectral function can be decomposed with the projection operators $\Lambda_\pm(\boldsymbol{p}) = (1\pm\gamma_0\hat{\boldsymbol{p}}\cdot\boldsymbol{\gamma})/2$ as

$$\rho(\nu,\boldsymbol{p}) = \rho_+(\nu,p)\Lambda_+(\boldsymbol{p})\gamma_0 + \rho_-(\nu,p)\Lambda_-(\boldsymbol{p})\gamma_0, \tag{8}$$

with $p=|\boldsymbol{p}|$, $\hat{\boldsymbol{p}}=\boldsymbol{p}/p$, and

$$\rho_\pm(\nu,p) = \frac{1}{2}\mathrm{Tr}_D[\rho(\nu,\boldsymbol{p})\gamma_0\Lambda_\pm(\boldsymbol{p})]. \tag{9}$$

It is shown from the anticommutation relations of ψ and $\bar\psi$ that the decomposed spectral functions satisfy the sum rules,

$$\int d\nu\rho_\pm(\nu,p) = 1. \tag{10}$$

Using charge conjugation symmetry, one can show that $\rho_\pm(\nu,\boldsymbol{p})$ satisfy [23]

$$\rho_\pm(\nu,p) = \rho_\mp(-\nu,p). \tag{11}$$

On the lattice, one can measure the imaginary-time correlator Eq. (4) for discrete imaginary times. To obtain the quark propagator, one has to deduce the spectral function from this information. In Refs. [21–23], the quark correlator in Landau gauge is analyzed on the lattice with the quenched approximation, and the quark spectral function is analyzed with the two-pole *Ansatz*,

$$\rho_+(\nu,p) = Z_+(p)\delta(\nu-\nu_+(p)) + Z_-(p)\delta(\nu+\nu_-(p)), \tag{12}$$

where $Z_\pm(p)$ and $\nu_\pm(p)$ are the residues and positions of the poles, respectively. The four parameters, $Z_\pm(p)$ and $\nu_\pm(p)$, are determined by fitting the correlators obtained on the lattice for each p.

Some comments on the two-pole fit in Refs. [21–23] are in order. First, the two poles in Eq. (12) at $\nu_+(p)$ and $\nu_-(p)$, respectively, correspond to the normal and plasmino modes in the HTL approximation. In fact, the study of the momentum and bare quark mass, m_0, dependences of the fitting parameters [21–23] shows that the behavior of these parameters is consistent with this observation [24,26]; for example, for large m_0 or p the residue of the plasmino mode $Z_-(p)$ becomes small, and the propagator approaches that of the free quark. Second, the restoration of the chiral symmetry for massless quarks above T_c is checked explicitly on the lattice by measuring the scalar term in the massless quark propagator [21,23]. Third, in Refs. [21,23] the extension of the fitting *Ansatz* to allow for the width of the poles is also performed. It, however, is found that the χ^2 of this fit always has a minimum for vanishing widths, and this extension does not improve the fit. This result indicates that the existence of sharp quasiparticle peaks in the quark spectral function even near T_c is supported from the lattice analysis.

In Fig. 2, we show the fitting result of each parameter in Eq. (12) for massless quarks as a function of p for $T=1.5T_c$ and $3T_c$ obtained in Ref. [23]. These analyses are performed on the lattice with the volume $128^3\times16$, where both the lattice spacing and finite volume effects are found to be small [23]. In the upper panel, p dependences of $\nu_\pm(p)$, i.e., the dispersion relations of the normal and plasmino modes, are shown by the open symbols. The vertical and horizontal axes are normalized by the thermal mass m_T defined by the value of $\nu_\pm(p)$ at $p=0$: The value of m_T obtained on the lattice after the extrapolation to the infinite volume limit is $m_T/T = 0.768(11)$ and $0.725(14)$

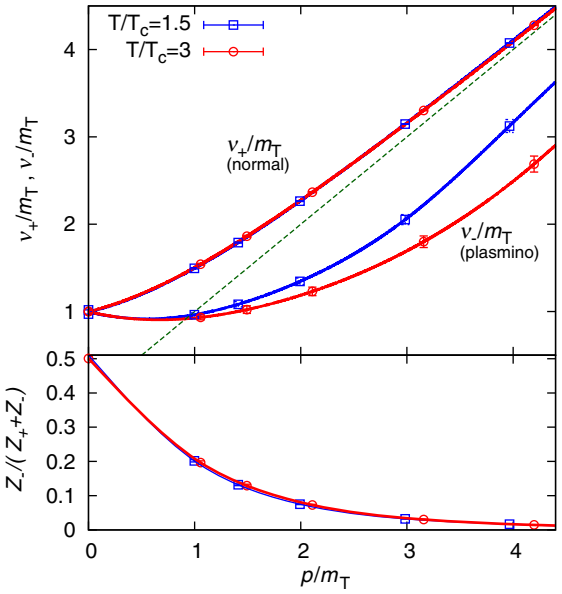

FIG. 2 (color online). Open symbols show the momentum dependence of the parameters $\nu_+(p)$, $\nu_-(p)$ and $Z_-(p)/(Z_+(p)+Z_-(p))$ obtained on the lattice in Ref. [23]. The solid lines represent their interpolation obtained by the cubic spline method. The dashed line represents the light cone.

at $T = 1.5T_c$ and $3T_c$, respectively [23]. The lower panel shows the relative weight of the plasmino residue, $Z_-/(Z_+ + Z_-)$. This figure shows that the weight becomes smaller as p increases, which indicates that the quark propagator for large p/T is dominated by the normal mode. A result similar to that shown in Fig. 2 is obtained by the Schwinger-Dyson approach for the quark propagator [27].

The above results are obtained in quenched approximation. In full QCD, the form of the quark spectrum may be altered due to contributions of dynamical quark loops. It should also be noted that the T_c in the quenched approximation is estimated about 1.5 times larger than that of full QCD.

Although the lattice data are available only for discrete values of p, we must have the quark propagator as a continuous function of p to solve the SDE. For this purpose, we take the interpolation and extrapolation of the lattice data by the cubic spline method. From the charge conjugation symmetry, one can show that $\mathrm{d}\nu_+(p)/\mathrm{d}p = -\mathrm{d}\nu_-(p)/\mathrm{d}p$, $\mathrm{d}^2\nu_+(p)/\mathrm{d}p^2 = \mathrm{d}^2\nu_-(p)/\mathrm{d}p^2$, and $Z_+(p) = Z_-(p)$ for $p = 0$ [22,23]. These properties are taken into account in our cubic spline interpolation. The lattice data are available only in the momentum range $p/T \lesssim 4.7$. To take extrapolations to higher momenta, we extrapolate the parameters using an exponentially damping form for $Z_-/(Z_+ + Z_-)$,

$$Z_-/(Z_+ + Z_-) = R\mathrm{e}^{-\alpha p}, \tag{13}$$

and $\nu_\pm(p)$ are extrapolated by functions,

$$\nu_\pm(p) = p + \beta_1^\pm \mathrm{e}^{-\beta_2^\pm p}, \tag{14}$$

which exponentially approach the light cone for large p. The parameters R, α, and $\beta_i^\pm$ are determined in the cubic spline analysis. The p dependence of each parameter determined in this way is shown by the solid lines in Fig. 2. We tested another extrapolation form by a polynomial, $\nu_\pm(p) = p + \beta_1'^\pm/p + \beta_2'^\pm/p^2 + \cdots$, but found that it hardly changes the dispersion relation. Finally, we fix

$$Z_+ + Z_- = 1 \tag{15}$$

throughout this paper to satisfy the sum rule Eq. (10). We note that the slope of the plasmino dispersion relation exceeds unity for $p \gtrsim 3m_T$ and is acausal. This unphysical behavior may come from an artifact of the lattice simulation and/or the *Ansatz* for the spectral function. However, the residue of the plasmino mode is small, $Z_-(p) < 0.05$, in this momentum region, and the contribution of this branch in this momentum range to our final result is well suppressed.

With the two-pole form of the spectral function in Eq. (12), the quark propagator reads

$$\begin{aligned} S(i\nu_n, \boldsymbol{p}) &= S_+(i\nu_n, p)\Lambda_+(\boldsymbol{p})\gamma_0 + S_-(i\nu_n, p)\Lambda_-(\boldsymbol{p})\gamma_0, \\ &= \sum_{s=\pm} S_s(i\nu_n, p)\Lambda_s(\boldsymbol{p})\gamma_0, \end{aligned} \tag{16}$$

where

$$S_s(i\nu_n, p) = \frac{Z_+(p)}{i\nu_n - s\nu_+(p)} + \frac{Z_-(p)}{i\nu_n + s\nu_-(p)}. \tag{17}$$

The symbols $s = \pm$ on the right-hand side are understood as the numbers ± 1. Correspondingly, the inverse propagator is given by

$$S^{-1}(i\nu_n, \boldsymbol{p}) = \sum_{s=\pm} S_s^{-1}(i\nu_n, p)\gamma_0\Lambda_s(\boldsymbol{p}), \tag{18}$$

with

$$S_s^{-1}(i\nu_n, p) = \frac{(i\nu_n - s\nu_+(p))(i\nu_n + s\nu_-(p))}{i\nu_n - sE(p)} \tag{19}$$

and

$$E(p) = -Z_+(p)\nu_-(p) + Z_-(p)\nu_+(p). \tag{20}$$

Note that the inverse propagator has poles at $i\nu_n = \pm E(p)$. These poles inevitably appear in the multipole *Ansatz*, because the propagator Eq. (17) has one zero point in the range of ω surrounded by two poles. The form of the inverse propagator Eq. (19) will be used in the construction of the vertex function. We will see that the poles at $i\nu_n = \pm E(p)$ give rise to additional terms in the dilepton production rate.

C. Vertex function

The SDE, Eq. (2), requires the full photon-quark vertex $\Gamma_\mu(P+Q,P)$ besides the full quark propagator. So far, the evaluation of $\Gamma_\mu(P+Q,P)$ on the lattice at nonzero temperature has not been performed to the best of the authors' knowledge. In the present study, we construct the vertex function from the lattice quark propagator respecting the Ward-Takahashi identity (WTI) as follows.

The gauge invariance requires that the vertex function must fulfill the WTI,

$$Q_\mu \Gamma^\mu(P+Q,P) = S^{-1}(P+Q) - S^{-1}(P), \tag{21}$$

with the inverse quark propagator $S^{-1}(P)$. For $\boldsymbol{q}=0$, the temporal component Γ_0 is completely determined only by this constraint as follows. First, in this case $\boldsymbol{q}\cdot\boldsymbol{\Gamma}$ should vanish, provided that Γ_i $(i=1,2,3)$ are not singular at $\boldsymbol{q}=0$. Then, by substituting $\boldsymbol{q}\cdot\boldsymbol{\Gamma}=0$ in Eq. (21), one obtains

$$\Gamma_0(i\omega_m + i\nu_n, \boldsymbol{p}; i\nu_n, \boldsymbol{p}) = \frac{1}{i\omega_m}[S^{-1}(i\omega_m + i\nu_n, \boldsymbol{p}) - S^{-1}(i\nu_n, \boldsymbol{p})]. \tag{22}$$

On the other hand, the spatial components Γ_i cannot be determined only with Eq. (21) [28]. In the present study, we employ an approximation to neglect the $\boldsymbol{q}$ dependence of $\Gamma_0(i\omega_m + i\nu_n, \boldsymbol{p}+\boldsymbol{q}; i\nu_n, \boldsymbol{p})$ at $\boldsymbol{q}=0$. In other words, we assume that

$$\partial\Gamma_0(i\omega_m + i\nu_n, \boldsymbol{p}+\boldsymbol{q}; i\nu_n, \boldsymbol{p})/\partial q_i|_{\boldsymbol{q}=0} = 0. \tag{23}$$

With this approximation and Eq. (21), one obtains

$$q^i\Gamma_i(i\omega_m + i\nu_n, \boldsymbol{p}+\boldsymbol{q}; i\nu_n, \boldsymbol{p}) = S^{-1}(i\omega_m + i\nu_n, \boldsymbol{p}+\boldsymbol{q}) - S^{-1}(i\omega_m + i\nu_n, \boldsymbol{p}). \tag{24}$$

By taking the leading-order terms in $\boldsymbol{q}$ on both sides, one has

$$\begin{aligned}\Gamma_i(i\omega_m + i\nu_n, \boldsymbol{p}; i\nu_n, \boldsymbol{p}) &= \frac{\partial S^{-1}}{\partial p^i}(i\omega_m + i\nu_n, \boldsymbol{p}) \\ &= \sum_{s=\pm}\frac{\partial S_s^{-1}(i\omega_m + i\nu_n, p)}{\partial p^i}\gamma_0\Lambda_s(\boldsymbol{p}) \\ &\quad + \sum_{s=\pm} S_s^{-1}(i\omega_m + i\nu_n, p)\gamma_0\frac{\partial\Lambda_s(\boldsymbol{p})}{\partial p^i},\end{aligned} \tag{25}$$

where in the second equality, we used Eq. (18).

We note that there is no *a priori* justification of Eq. (23). By expanding Γ_0 with respect to $\boldsymbol{q}$ at $\boldsymbol{q}=0$, one obtains

$$\begin{aligned}i\omega_m\Gamma_0(i\omega_m + i\nu_n, \boldsymbol{p}+\boldsymbol{q}; i\nu_n, \boldsymbol{p}) &= S^{-1}(i\omega_m + i\nu_n, \boldsymbol{p}) - S^{-1}(i\nu_n, \boldsymbol{p}) \\ &\quad + \boldsymbol{q}\cdot\boldsymbol{p}\gamma_0 A(i\omega_m + i\nu_n, i\nu_n, \boldsymbol{p}^2) \\ &\quad + (\boldsymbol{q}\cdot\boldsymbol{p})(\hat{\boldsymbol{p}}\cdot\boldsymbol{\gamma})B(i\omega_m + i\nu_n, i\nu_n, \boldsymbol{p}^2) \\ &\quad + \boldsymbol{q}\cdot\boldsymbol{\gamma}C(i\omega_m + i\nu_n, i\nu_n, \boldsymbol{p}^2) + O(\boldsymbol{q}^2),\end{aligned} \tag{26}$$

where A, B, and C are unknown functions. Our approximation corresponds to neglecting these functions. Although these functions do not affect Eq. (22) at $\boldsymbol{q}=0$, the corresponding terms appear in Eq. (25) when these functions are nonzero. The determination of the nonperturbative form of the photon-quark and gluon-quark vertices is generally difficult, and various approximations have been employed in studies of the SDE [28–31]. It should be emphasized that the vertex functions, Eqs. (22) and (25), satisfy the WTI and thus are advantageous in light of the gauge invariance among various ansätze on the vertex function. Γ_0, in Eq. (22), is the same as that obtained in Ref. [28] since it is uniquely determined only from the WTI. On the other hand, Γ_i differ from the ones in Ref. [28], even when only the longitudinal part in Ref. [28] is concerned. Introduction of the functions given in Eq. (26) fills this difference. We, however, left the analysis of the dependences of our result on these functions to future study. Here we just emphasize that there exist infinite choices of these functions because there is no guiding principle to determine these functions. The other comment on the vertex function, Eqs. (22) and (25), is that this vertex function can be continuously extended to nonzero $\boldsymbol{q}$ in a simple way. The analysis of the invariant mass distribution of the dilepton production rate and the real-photon production rate with the vertex function will be reported in a future publication [32].

III. DILEPTON PRODUCTION RATE

The goal of the present study is to obtain the dilepton production rate with the lattice quark propagators and the vertex function discussed in the previous section. In this section, however, before the analysis of the full manipulation, we first see the dilepton production rates in simpler cases: (1) the free quark gas in Sec. III A and (2) the case with the lattice quark propagators but with the bare vertex function in Sec. III B. The full analysis is then presented in Sec. III C.

A. Free quark gas

The photon self-energy for the massless free quark gas is obtained by substituting the free quark propagator $S(i\nu_n,\boldsymbol{p}) = 1/(i\nu_n\gamma_0 - \boldsymbol{p}\cdot\boldsymbol{\gamma})$ and bare vertex function $\Gamma_\mu = \gamma_\mu$ into Eq. (2). The result of the dilepton production rate for the massless two-flavor case is given by [26]

$$\left.\frac{d\Gamma}{d\omega d^3q}\right|_{q=0} = \frac{5\alpha^2}{36\pi^4}\left(f\left(\frac{\omega}{2}\right)\right)^2, \tag{27}$$

where $f(\omega) = 1/(e^{\beta\omega}+1)$ is the Fermi distribution function.

B. Dilepton production rate without vertex correction

Next, we calculate the photon self-energy and the dilepton production rate with the lattice quark propagators from Eq. (16) but with $\Gamma_\mu = \gamma_\mu$. The photon self-energy obtained in this way, of course, does not fulfill the gauge invariance. The result obtained here, however, is helpful in understanding the effect of the vertex correction, i.e., the role of the WTI.

The photon self-energy with the bare vertex is given by

$$\Pi_{\mu\nu}(i\omega_m, \boldsymbol{q}) = -\frac{5e^2}{3}T\sum_n\int\frac{d^3p}{(2\pi)^3} \times \mathrm{Tr}_D[S(i\nu_n,\boldsymbol{p})\gamma_\mu S(i\omega_m+i\nu_n,\boldsymbol{p}+\boldsymbol{q})\gamma_\nu]. \tag{28}$$

By substituting Eq. (16) into this formula, we obtain

$$\Pi_{\mu\nu}(i\omega_m, \boldsymbol{0}) = -\frac{5e^2}{3}T\sum_n\int\frac{d^3p}{(2\pi)^3} \times\sum_{s,t=\pm}S_s(i\nu_n,p)S_t(i\omega_m+i\nu_n,p) \times\mathrm{Tr}_D[\Lambda_s\gamma_0\gamma_\mu\Lambda_t\gamma_0\gamma_\nu]. \tag{29}$$

The trace in Eq. (29) is calculated with

$$\mathrm{Tr}_D[\Lambda_s(\boldsymbol{p})\Lambda_t(\boldsymbol{p})] = 2\delta_{st}, \tag{30}$$

$$\mathrm{Tr}_D[\Lambda_s(\boldsymbol{p})\gamma_0\gamma_i\Lambda_t(\boldsymbol{p})\gamma_0\gamma_i] = 2\delta_{s,-t} + 2st\hat{p}_i^2, \tag{31}$$

where it is understood that

$$\delta_{++} = \delta_{--} = 1, \qquad \delta_{+-} = \delta_{-+} = 0, \tag{32}$$

$$\delta_{s,-t} = \delta_{s,\mp} \quad (\text{for } t = \pm). \tag{33}$$

Substituting Eqs. (30), (31), and $\sum_i\hat{p}_i^2 = 1$ into Eq. (29), one obtains

$$\Pi_\mu^\mu(i\omega_m, \boldsymbol{0}) = \frac{20e^2}{3}T\sum_n\int\frac{d^3p}{(2\pi)^3} \times\sum_{s=\pm}S_s(i\nu_n,p)S_{-s}(i\omega_m+i\nu_n,p), \tag{34}$$

where

$$S_{-s}(i\nu_n+i\omega_m,p) = S_\mp(i\nu_n+i\omega_m,p)(\text{for } s=\pm). \tag{35}$$

Using Eq. (17) and taking the Matsubara sum and the analytic continuation $i\omega_m \to \omega + i\eta$, we obtain

$$\Pi_\mu^{R,\mu}(\omega,\boldsymbol{0}) = \frac{-40\alpha}{3\pi}\int_0^\infty dpp^2\left\{\frac{Z_+(p)^2(1-2f(\nu_+(p)))}{\omega-2\nu_+(p)+i\eta} + \frac{Z_-(p)^2(1-2f(\nu_-(p)))}{\omega-2\nu_-(p)+i\eta} + \frac{2Z_+(p)Z_-(p)(f(\nu_-(p))-f_+(\nu_+(p)))}{\omega-\nu_+(p)+\nu_-(p)+i\eta}\right\}. \tag{36}$$

Taking the imaginary part of this result, we have

$$\begin{aligned}\mathrm{Im}\Pi_\mu^{R,\mu}(\omega,\boldsymbol{0}) &= \frac{40\alpha}{3}\int_0^\infty dpp^2\{Z_+(p)^2\delta(\omega-2\nu_+(p))(1-2f(\nu_+(p))) \\ &+ Z_-(p)^2\delta(\omega-2\nu_-(p))(1-2f(\nu_-(p))) \\ &+ 2Z_+(p)Z_-(p)\delta(\omega-\nu_+(p)+\nu_-(p)) \\ &\times(f(\nu_-(p))-f(\nu_+(p)))\}.\end{aligned} \tag{37}$$

The imaginary part of the photon self-energy is the difference between the annihilation and production rates of virtual photons in medium. The three terms in Eq. (37) represent different annihilation and production processes of a virtual photon. The first and second terms in Eq. (37) represent the production of a virtual photon through the pair annihilation of two normal modes and two plasmino modes, respectively, which are diagrammatically shown in Fig. 3(a), and their inverse processes. This can be checked from the arguments of the δ functions and thermal factors in Eq. (37). The δ function in these terms represents the energy conservation in these processes, and the thermal factor which is rewritten as

$$1\text{–}2f(\omega) = (1-f(\omega))^2 - f(\omega)^2 \tag{38}$$

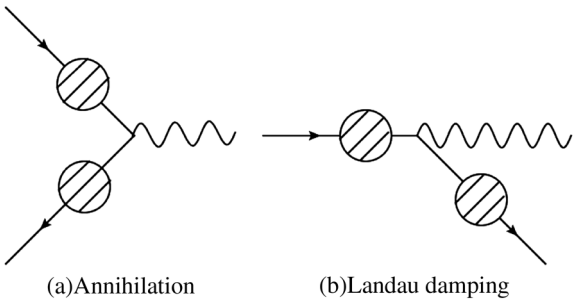

FIG. 3. Photon production processes.

is the difference between the products of the Pauli blocking effects and thermal distributions. The existence of the residues $Z_\pm(p)$ in these terms is similarly understood. The last term in Eq. (37) represents the Landau damping between normal and plasmino modes, which is diagrammatically shown in Fig. 3(b). Correspondingly, the thermal factor in this term can be rewritten as

$$f(\omega_1)-f(\omega_2)=f(\omega_1)(1-f(\omega_2))-f(\omega_2)(1-f(\omega_1)). \tag{39}$$

The δ functions in Eq. (37) can be integrated out. The form of the dilepton production rate after the integration over p reads

$$\mathrm{Im}\Pi^{R,\mu}_\mu(\omega,\mathbf{0})=\frac{40\alpha}{3}\left\{\frac{p^2Z_+(p)^2}{2|d\nu_+(p)/dp|}(1-2f(\nu_+(p)))|_{\omega=2\nu_+(p)}+\sum_l\frac{p_l^2Z_-(p_l)^2}{2|d\nu_-(p_l)/dp|}(1-2f(\nu_-(p_l)))|_{\omega=2\nu_-(p_l)}\right.$$
$$\left.+\sum_l\frac{2p_l^2Z_+(p_l)Z_-(p_l)}{|d[\nu_+(p_l)-\nu_-(p_l)]/dp|}(f(\nu_-(p_l))-f(\nu_+(p_l)))|_{\omega=\nu_+(p_l)-\nu_-(p_l)}\right\}, \tag{40}$$

where the momentum p in each term is given by the condition arising from the δ functions in Eq. (37). Each term can take nonzero values only when there exist momenta satisfying this condition for a given ω. This gives the condition for ω at which each term takes a nonzero value. For example, the first term takes nonzero values for $\omega>2m_\mathrm{T}$. Because the second and third terms can have multiple solutions of p for a fixed ω, we represent this possibility by the sum over l. It is also notable that each term in Eq. (40) is inversely proportional to the derivative of $\nu_\pm(p)$ and $\nu_+(p)-\nu_-(p)$; they come from the density of states of each modes. Accordingly, the dilepton production rate diverges when the derivatives vanish. Such divergence is known as van Hove singularity. In Sec. IV, we will see the appearance of such singularities in the dilepton spectrum.

C. Dilepton production rate with vertex correction

Now, let us calculate the dilepton production rate with the lattice quark propagator in Eq. (16) and the full vertex functions in Eqs. (22) and (25).

When the full vertex function satisfying the WTI is used in Eq. (2), the temporal component Π_{00} for $\boldsymbol{q}=0$ vanishes. One can easily check this explicitly by substituting Eq. (22) into Eq. (2). For $\sum_{i=1}^3\Pi_{ii}$, by substituting Eqs. (16) and (25) into Eq. (2), one has

$$\sum_{i=1}^3\Pi_{ii}(i\omega_m,\mathbf{0})=\frac{5e^2}{3}T\sum_n\int\frac{d^3p}{(2\pi)^3}\sum_{s,t,u=\pm}S_s(i\nu_n,p)S_t(i\nu_n+i\omega_m,p)$$
$$\times\sum_{i=1}^3\left(\hat{p}_i\frac{\partial S_u^{-1}(i\nu_n+i\omega_m,p)}{\partial p}\mathrm{Tr}_\mathrm{D}[\Lambda_s\gamma_0\gamma_i\Lambda_t\Lambda_u]+\frac{uS_u^{-1}(i\nu_n+i\omega_m,p)}{2p}\mathrm{Tr}_\mathrm{D}[\Lambda_s\gamma_0\gamma_i\Lambda_t\gamma_0(\gamma_i-(\hat{\boldsymbol{p}}\cdot\boldsymbol{\gamma})\hat{p}_i)]\right). \tag{41}$$

We substitute the following relations for the Dirac traces,

$$\mathrm{Tr}_\mathrm{D}[\Lambda_s\gamma_0\gamma_i\Lambda_t\Lambda_s]=2s\hat{p}_i\delta_{st}\delta_{tu}, \tag{42}$$

$$\mathrm{Tr}_\mathrm{D}[\Lambda_s\gamma_0\gamma_i\Lambda_t\gamma_0\gamma_i]=2\delta_{s,-t}+2st\hat{p}_i^2, \tag{43}$$

$$\mathrm{Tr}_\mathrm{D}[\Lambda_s\gamma_0\gamma_i\Lambda_t\gamma_0(\hat{\boldsymbol{p}}\cdot\boldsymbol{\gamma})]=2\hat{p}_i\delta_{st}, \tag{44}$$

and obtain

$$\sum_i\Pi_{ii}(i\omega_m,\mathbf{0})=\frac{10e^2}{3}T\sum_n\int\frac{d^3p}{(2\pi)^3}\sum_{s=\pm}sS_s(i\nu_n,p)$$
$$\times\left\{\frac{\partial\ln S_s^{-1}(i\nu_n+i\omega_m,p)}{\partial p}-\frac{1}{p}\left(1-\frac{S_{-s}(i\nu_n+i\omega_m,p)}{S_s(i\nu_n+i\omega_m,p)}\right)\right\}, \tag{45}$$

where to obtain the first term we used

$$S_s(i\nu_n,p)\frac{\partial S_s^{-1}(i\nu_n,p)}{\partial p}=\frac{\partial\ln S_s^{-1}(i\nu_n,p)}{\partial p}. \tag{46}$$

Up to now, the calculation relies only on the decomposition in Eq. (16), which is valid for the chiral symmetric quark propagator, and the form for the vertex in Eq. (25). The result in Eq. (45), thus, is valid for any form of the quark propagator $S_\pm(i\nu_n, p)$. Now we use the two-pole form of the quark propagator in Eqs. (17) and (19). The term including $\partial \ln S_s^{-1}/\partial p$ in Eq. (45) is then calculated to be

$$\begin{aligned}
&T\sum_n sS_s(i\nu_n,p)\frac{\partial \ln S_s^{-1}(i\nu_n+i\omega_m,\boldsymbol{p})}{\partial p}\\
&=-T\sum_n\left(\frac{Z_+}{i\nu_n-s\nu_+}+\frac{Z_-}{i\nu_n+s\nu_-}\right)\left(\frac{d\nu_+/dp}{i\nu_n+i\omega_m-s\nu_+}-\frac{d\nu_-/dp}{i\nu_n+i\omega_m+s\nu_-}-\frac{dE/dp}{i\nu_n+i\omega_m-sE}\right)\\
&=-\left(\frac{Z_+d\nu_-/dp}{i\omega_m+s\nu_++s\nu_-}+\frac{Z_-d\nu_+/dp}{i\omega_m-s\nu_+-s\nu_-}\right)(f(s\nu_+)+f(s\nu_-)-1)\\
&\quad-\frac{Z_+dE/dp}{i\omega_m+s\nu_+-sE}(f(s\nu_+)-f(sE))-\frac{Z_-dE/dp}{i\omega_m-s\nu_--sE}(f(s\nu_-)-f(sE)),
\end{aligned}\tag{47}$$

where the Matsubara sum over n is taken in the last equality. The remaining part of Eq. (45) is calculated as follows:

$$\begin{aligned}
&T\sum_n sS_s(i\nu_n,p)\left(1-\frac{S_{-s}(i\nu_n+i\omega_m,p)}{S_s(i\nu_n+i\omega_m,p)}\right)\frac{1}{p}\\
&=T\sum_n\left(\frac{Z_+}{i\nu_n-s\nu_+}+\frac{Z_-}{i\nu_n+s\nu_-}\right)\\
&\quad\times\left(\frac{F_1}{i\nu_n+i\omega_m-sE}+\frac{F_2}{i\nu_n+i\omega_m+s\nu_+}+\frac{F_3}{i\nu_n+i\omega_m-s\nu_-}\right)
\end{aligned}\tag{48}$$

$$\begin{aligned}
&=\frac{Z_+F_1}{i\omega_m+s\nu_+-sE}(f(sE)-f(s\nu_+))+\frac{Z_-F_1}{i\omega_m-s\nu_--sE}(f(sE)-f(-s\nu_-))\\
&\quad+\frac{Z_+F_2}{i\omega_m+2s\nu_+}(f(-s\nu_+)-f(s\nu_+))+\frac{Z_-F_2}{i\omega_m+s\nu_+-s\nu_-}(f(-s\nu_+)-f(-s\nu_-))\\
&\quad+\frac{Z_+F_3}{i\omega_m+s\nu_+-s\nu_-}(f(s\nu_-)-f(s\nu_+))+\frac{Z_-F_3}{i\omega_m-2s\nu_-}(f(s\nu_-)-f(-s\nu_-)),
\end{aligned}\tag{49}$$

where

$$F_1=-\frac{2E(\nu_-+E)(\nu_+-E)}{p(\nu_--E)(\nu_++E)},\quad F_2=\frac{2\nu_+(\nu_+-E)(\nu_+-\nu_-)}{p(\nu_++E)(\nu_++\nu_-)},\quad F_3=\frac{2\nu_-(\nu_+-\nu_-)(\nu_-+E)}{p(\nu_++\nu_-)(\nu_--E)}.$$

Here, each combination of $\nu_\pm$ and E in the parantheses is set to become positive; this can be checked by the relation $\nu_+>\nu_->-E>0$.

Combining these results, Eq. (45) is calculated to be

$$\begin{aligned}
\sum_{i=1}^{3}\Pi_{ii}(i\omega_m,\mathbf{0})=&-\frac{10e^2}{3}\int\frac{d^3p}{(2\pi)^3}\sum_{s=\pm}s\left\{\frac{2Z_+^2\nu_+\bar\Omega}{p(\nu_++E)}\frac{1-2f(\nu_+)}{i\omega_m+2s\nu_+}+\frac{2Z_-^2\nu_-\bar\Omega}{p(\nu_--E)}\frac{1-2f(\nu_-)}{i\omega_m+2s\nu_-}\right.\\
&+2Z_+Z_-\bar\Omega\frac{\bar\Omega E-2\omega_+\omega_-}{p(\nu_++E)(\nu_--E)}\frac{f(\nu_-)-f(\nu_+)}{i\omega_m-s\nu_++s\nu_-}\\
&-\left(Z_+\frac{d\nu_-}{dp}-Z_-\frac{d\nu_+}{dp}\right)\frac{1-f(\nu_+)-f(\nu_-)}{i\omega_m+s\nu_++s\nu_-}\\
&\left.+\left(-\frac{2Z_+Z_-E(\nu_++\nu_-)^2}{p(\nu_++E)(\nu_--E)}-\frac{dE}{dp}\right)\left(Z_+\frac{f(E)-f(\nu_+)}{i\omega_m+s\nu_+-sE}+Z_-\frac{f(-E)-f(\nu_-)}{i\omega_m+s\nu_--sE}\right)\right\}
\end{aligned}\tag{50}$$

with $\bar\Omega=\nu_+-\nu_-$.

By taking the analytic continuation $i\omega_m \to \omega + i\eta$, and taking the imaginary part, we obtain

$$\begin{aligned}\mathrm{Im}\Pi_\mu^{R,\mu}(\omega,\mathbf{0}) = -\frac{20\alpha}{3}\int dp p^2\Bigg[-\frac{2\bar{\Omega}}{p}\Bigg\{\frac{Z_+^2\nu_+}{\nu_+ + E}(1-2f(\nu_+))\delta(\omega-2\nu_+) + \frac{Z_-^2\nu_-}{\nu_- - E}(1-2f(\nu_-))\delta(\omega-2\nu_-) \\ -Z_+Z_-\frac{\bar{\Omega}E - 2\nu_+\nu_-}{(\nu_+ + E)(\nu_- - E)}(f(\nu_-)-f(\nu_+))\delta(\omega-\nu_+ + \nu_-)\Bigg\} \\ + \left(Z_+\frac{d\nu_-}{dp} - Z_-\frac{d\nu_+}{dp}\right)(1-f(\nu_+)-f(\nu_-))\delta(\omega-\nu_+-\nu_-) \\ + \left(\frac{2Z_+Z_-E(\nu_+ + \nu_-)^2}{p(\nu_+ + E)(\nu_- - E)} + \frac{dE}{dp}\right) \\ \times\{Z_+(1-f(-E)-f(\nu_+))\delta(\omega-\nu_+ + E) + Z_-(f(-E)-f(\nu_-))\delta(\omega-\nu_- - E)\}\Bigg] \\ + (\omega\to-\omega). \end{aligned} \tag{51}$$

Now let us inspect the physical meaning of each term in Eq. (51). From the δ functions and thermal factors, one finds that the two terms in the first line represent the pair creation and annihilation processes of normal and plasmino modes, respectively. The second line corresponds to the Landau damping. These terms have corresponding counterparts in Eq. (37), although the coefficients of these terms are modified by the vertex correction. The term in the third line in Eq. (51) can be interpreted as the pair annihilation and creation of a normal mode and a plasmino one. This process does not appear in Eq. (37) and can manifest itself as a consequence of the vertex correction. We note that a similar process exists in the formula obtained in Ref. [12]. In this way, the terms in the first three lines in Eq. (51) can be understood as the annihilation, creation, and scattering processes of quark quasiparticles. We also note that the Landau damping of two normal or two plasmino modes does not exist in Eq. (51) because such a process can exist only for $\omega = 0$ at $\boldsymbol{q} = 0$.

On the other hand, one cannot give such interpretations to the terms in the fourth and fifth lines in Eq. (51). From the δ functions and the thermal factors, these terms seem to represent the decay and creation rates with a quasiparticle mode with energy $\pm E$, which, however, does not exist in the quark propagator in Eq. (17). Mathematically, these terms come from the poles in the vertex function in Eq. (25). The poles appear in the vertex function via the WTI in Eq. (21) and the fact that the analytic continuation of the propagator $S_s(i\nu_n, p)$ gives zero points at energies $\pm E$. As discussed in Sec. II B, the zero in $S_s(\omega, p)$ inevitably appears between the two poles in the two-pole form of the quark propagator Eq. (17).

Another remark on Eq. (51) is the sign of each term in Eq. (51). In Eq. (51), all terms are separately positive definite for $\omega > 0$ except for the one in the third line, which becomes negative for sufficiently large ω. The negative contribution of this term is, however, canceled out by the last term; we have checked that the sum of these terms is always positive. The total dilepton production rate for $\omega > 0$, therefore, takes a positive value as it should.

In Fig. 4, we show the dispersion relation of $E(p)$ for $T = 1.5T_c$. For $p = 0$, $E(p)$ vanishes because of chiral symmetry, while $-E(p)$ approaches p for large p. The figure shows that $-E(p)$ is a monotonically increasing function of p. The result for $T = 3T_c$ is qualitatively the same. In Fig. 4, we also show the combinations of the dispersion relations appearing in the δ functions in Eq. (51),

$$\nu_+ + \nu_-, \qquad \nu_+ - \nu_-, \qquad \nu_+ - E, \qquad \nu_- + E. \tag{52}$$

From the figure, one sees that $\nu_+ - E$ and $\nu_- + E$ are monotonically increasing and decreasing functions of p, respectively, starting from m_T at $p = 0$. Also, $\nu_+ - E > m_T$ and $0 < \nu_- + E < m_T$ are satisfied. These behaviors become transparent by rewriting these combinations as

$$\nu_+ - E = Z_+(\nu_+ + \nu_-), \tag{53}$$

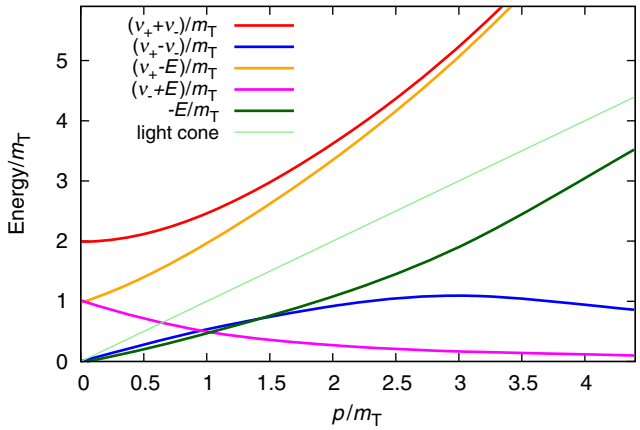

FIG. 4 (color online). Momentum dependences of various functions composed of $\nu_\pm(p)$ and E.

$$\nu_- + E = Z_-(\nu_+ + \nu_-), \tag{54}$$

where we used Eq. (20).

We finally comment on the limiting behaviors of Eq. (51). First, in our two-pole *Ansatz* the quark propagator for massless free quarks is obtained by setting

$$Z_+(p) = 1, \qquad Z_-(p) = 0, \qquad \nu_+(p) = p. \tag{55}$$

Equation (51), thus, should reproduce the photon self-energy of the free quark gas, when Eq. (55) is substituted. This can be explicitly checked as follows. By substituting $Z_- = 0$, all terms including Z_- vanish. Since $E = -\nu_-$ for $Z_- = 0$, the third and fourth lines in Eq. (51) cancel out each other without constraints on $\nu_-(p)$. Only the first term in Eq. (51), thus, survives, which gives the free quark result. Second, our result on the dilepton production rate approaches the free quark one in the large ω limit because the lattice quark propagator used in this study reproduces Eq. (55) at large momentum. This behavior will be explicitly checked in the next section.

IV. NUMERICAL RESULTS

Now let us see the numerical results on the dilepton production rate obtained in the previous section. In Fig. 5, we present the ω dependence of the dilepton production rate for $T = 1.5T_c$. In the figure, we also plot the result without the vertex correction in Eq. (37), together with the rates obtained by the HTL calculation [12] and the free quark gas in Eq. (27). The value of the thermal mass m_T is taken from the result obtained on the lattice [23].

Figure 5 shows that the production rate with the lattice quark propagators has divergences at two energies, $\omega/m_T = \omega_1/m_T \simeq 1.1$ and $\omega/m_T = \omega_2/m_T \simeq 1.8$. For $\omega < \omega_1$, our result, as a whole, behaves similarly to the HTL one [12]; i.e., it increases as ω decreases, although our production rate is smaller than the perturbative one for small ω. Near ω_1, however, it shows a prominent enhancement and exceeds the latter. The region, where the large production rate is obtained, is located around m_T. Therefore, it is possible that the production yield obtained by integrating this rate has large enhancement below several hundred MeV, where the enhancement in the experimentally observed dilepton spectra at RHIC [4–6] exists. The rate has a discontinuity at $\omega = \omega_1$ and is significantly suppressed compared with Eq. (27) for $\omega_1 < \omega < \omega_2$. The rate has another discontinuity at $\omega = \omega_2$, above which the rate is close to the free quark one. In the dilepton rate without vertex correction, one also finds two divergences at $\omega = \omega_1$ and ω_2, while the rate vanishes for $\omega_1 < \omega < \omega_2$.

In order to understand these results in more detail, we show the contribution of each term in Eq. (51) separately in Fig. 6. In the figure, the rates coming from the pair annihilation of two normal modes (NN), two plasmino modes (PP), and a normal and a plasmino modes (NP) are separately shown, together with those of the Landau damping between quasiparticles (LD) and processes including an E mode with a normal (NE) and a plasmino (PE) mode. From the figure, one finds that the two divergences at $\omega = \omega_1$ and ω_2 come from the LD and PP rates, respectively. As discussed in Sec. III B, these divergences come from the van Hove singularity. The photon self-energy in Eq. (51) is inversely proportional to derivatives of the dispersion relations, $d\nu_-(p)/dp$ and $d\{\nu_+(p) - \nu_-(p)\}/dp$. As shown in Figs. 2 and 4, each of $\nu_-(p)$ and $\nu_+(p) - \nu_-(p)$ has an extremum at nonzero p. Their values at the extrema are $\nu_+(p) - \nu_-(p) = \omega_1$ and $2\nu_-(p) = \omega_2$. At these points, the derivatives vanish. This leads to the divergences in the photon self-energy and, accordingly, the dilepton production rate.

The divergences due to the van Hove singularity are buried if the quark quasiparticles have a width. When the width is not large, however, the enhancement of the

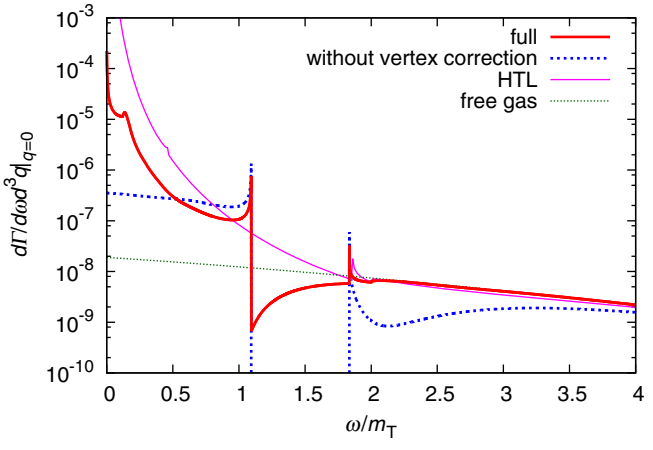

FIG. 5 (color online). Dilepton production rate at zero momentum for $T = 1.5T_c$. The result without vertex correction is also plotted. Thin lines represent the HTL and free quark results.

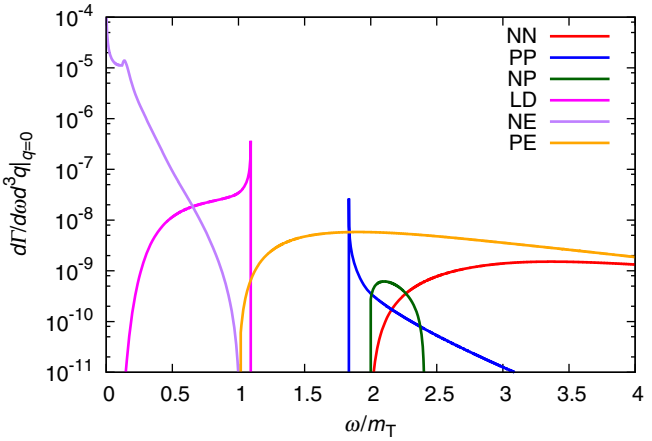

FIG. 6 (color online). Decomposition of the dilepton production rate.

dilepton production rate would be observed as a remnant of the van Hove singularity because the van Hove singularity takes place as a consequence of the concentration of the density of states. If the dispersion relation has a structure which causes such a concentration, the enhancement of the dilepton production rate is expected to occur although the singularity is blurred with the width of quasiparticles. It is also noteworthy that the analyses in Refs. [21,23] suggest the small width of quark quasiparticles as discussed already in Sec. II B. The enhancement of the dilepton production near $\omega \simeq m_T$ found in this study, therefore, can be a robust phenomenon with the modified dispersion relations of quark quasiparticles.

Figure 6 also shows that each individual process is nonvanishing in a limited range of ω. The range can be read off from the corresponding functions plotted in Fig. 4. The NN and NP rates are nonvanishing for $\omega > 2m_T$. On the other hand, the lower threshold of the PP rate, $\omega = \omega_2$, is slightly lower than $2m_T$, because $\nu_-(p)$ has a minimum smaller than m_T at nonzero momentum. The range of the Landau damping is also kinematically constrained to $\omega < \omega_1$. The NE and PE rates are nonvanishing for $\omega > m_T$ and $\omega < m_T$, respectively. The NE rate gives rise to a nonzero value for $\omega_1 < \omega < \omega_2$. To the dilepton production rate without the vertex correction, only the NN, PP, and LD contribute and the rate vanishes for $\omega_1 < \omega < \omega_2$.

For large ω, the rate is dominated by the NN. This is a consequence of the fact that the quark propagator approaches the free quark one as p becomes larger. A glance at Fig. 6 might give an impression that the NE rate also survives for large ω. Although not shown in Fig. 6, however, the NP rate takes a negative value for $\omega \gtrsim 2.4m_T$, and this term almost cancels out with the NE rate; see the discussion in Sec. III C.

Next, let us address the behavior of the production rate in the $\omega \to 0$ limit. The retarded photon self-energy is identical with the electromagnetic current-current correlation function,

$$J^R_{ij}(\omega, \boldsymbol{p}) = \int d^4x e^{i\omega t - i\boldsymbol{p}\cdot\boldsymbol{x}} \langle [j^{\mathrm{EM}}_i(t, \boldsymbol{x}), j^{\mathrm{EM}}_j(0, \boldsymbol{0})] \rangle \theta(t), \tag{56}$$

at the leading order in α. The low-energy behavior of $J^R_{ij}(\omega, \boldsymbol{p})$ is related to the electric conductivity σ through the Kubo formula,

$$\sigma = \frac{1}{6} \lim_{\omega \to 0} \frac{1}{\omega} \sum_{i=1}^{3} J^R_{ii}(\omega, \boldsymbol{0}). \tag{57}$$

Our result shows that $\sum_{i=1}^{3} J^R_{ii}(\omega, \boldsymbol{0})$ approaches zero faster than ω in the $\omega \to 0$ limit, and thus the electric conductivity vanishes. Incorporation of the width of the quasiparticle modes, which is not included in the form of the quark propagator used in this study, may lead to nonzero σ.

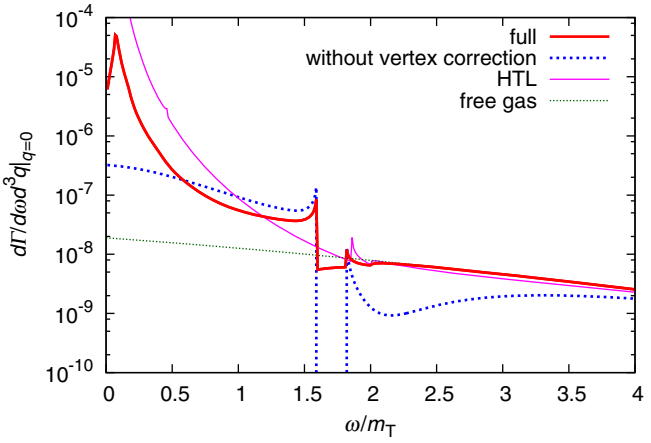

FIG. 7 (color online). Dilepton production rate from $3T_c$ deconfined phase.

In Fig. 7, we show the dilepton production rate at $T = 3T_c$. One sees that the behavior is qualitatively the same as the result for $T = 1.5T_c$. In particular, there exists an enhancement of the rate around $\omega \simeq 1.5m_T$ owing to the van Hove singularity. This indicates that the large enhancement of the dilepton production rate around $\omega \simeq m_T$ is a general result irrespective of T. The gap between ω_1 and ω_2 is narrower than that at $T = 1.5T_c$ because of the change of the dispersion relations $\nu_\pm(p)$ obtained on the lattice. One also finds that the rate takes a finite value at $\omega = 0$, while it diverges for $T = 1.5T_c$. This limiting behavior may depend on the way of the extrapolation of $\nu_\pm(p)$ to large momentum.

V. SUMMARY

In this study we have investigated the dilepton production rate using a quark propagator obtained on the lattice with a pole *Ansatz*. The Schwinger-Dyson equation for the photon self-energy is solved with the lattice quark propagator and the photon-quark vertex satisfying the Ward-Takahashi identity. The effect of the vertex correction is discussed by comparing the result with the calculation without vertex correction. Our numerical result shows that the dilepton production rate with the lattice quark propagators is larger by about one order or more compared with the one with free quark propagators in the low invariant mass region. Compared with the HTL result, there exists a significant enhancement around $\omega \simeq m_T \simeq T$ owing to the van Hove singularity. This result is interesting since such a large enhancement in the deconfined medium near T_c may explain the excess of the dilepton yield observed at PHENIX [4] in the low invariant mass region. To understand the effect of the enhancement of the dilepton rate on the experimental result quantitatively, the analysis with dynamical models describing the spacetime evolution of the hot medium and integration of the dilepton production rate is needed. Although in the present study we investigated the production rate with zero momentum, the three-momentum integrated production

rate is also needed for comparison with experiments. To obtain the three-momentum integrated production rate, the analysis carried out in this paper has to be extended to nonzero momentum. This will be reported elsewhere. In addition, a comparison with other nonperturbative approaches such as Ref. [33] will be the interesting focus of future work.

ACKNOWLEDGMENTS

The authors thank M. Harada for a useful comment on the vertex function. T. K. is supported by the Osaka University Cross-Boundary Innovation Program. This work is supported in part by JSPS KAKENHI Grants No. 23540307, No. 25800148, and No. 26400272.

[1] I. Arsene *et al.* (BRAHMS Collaboration), Nucl. Phys. **A757**, 1 (2005); B. B. Back *et al.* (PHOBOS Collaboration), *ibid.* **A757**, 28 (2005); J. Adams *et al.* (STAR Collaboration), *ibid.* **A757**, 102 (2005); K. Adcox *et al.* (PHENIX Collaboration), *ibid.* **A757**, 184 (2005).
[2] B. Muller, J. Schukraft, and B. Wyslouch, Annu. Rev. Nucl. Part. Sci. **62**, 361 (2012).
[3] R. Rapp, J. Wambach, and H. van Hees, Landolt-Bornstein **23**, 134 (2010).
[4] A. Adare *et al.* (PHENIX Collaboration), Phys. Rev. C **81**, 034911 (2010).
[5] J. Zhao (STAR Collaboration), J. Phys. G **38**, 124134 (2011).
[6] L. Adamczyk *et al.* (STAR Collaboration), Phys. Rev. Lett. **113**, 022301 (2014); **113**, 049903 (2014).
[7] L. D. McLerran and T. Toimela, Phys. Rev. D **31**, 545 (1985).
[8] H. A. Weldon, Phys. Rev. D **42**, 2384 (1990).
[9] C. Gale and J. I. Kapusta, Nucl. Phys. **B357**, 65 (1991).
[10] E. Braaten and R. D. Pisarski, Nucl. Phys. **B337**, 569 (1990).
[11] R. D. Pisarski, Nucl. Phys. **A525**, 175 (1991).
[12] E. Braaten, R. D. Pisarski, and T.-C. Yuan, Phys. Rev. Lett. **64**, 2242 (1990).
[13] S. M. H. Wong, Z. Phys. C **53**, 465 (1992).
[14] G. D. Moore and J.-M. Robert, arXiv:hep-ph/0607172.
[15] M. Laine, J. High Energy Phys. 11 (2013) 120.
[16] R. Rapp and J. Wambach, Adv. Nucl. Phys. **25**, 1 (2000).
[17] F. Karsch, E. Laermann, P. Petreczky, S. Stickan, and I. Wetzorke, Phys. Lett. B **530**, 147 (2002).
[18] H.-T. Ding, A. Francis, O. Kaczmarek, F. Karsch, E. Laermann, and W. Soeldner, Phys. Rev. D **83**, 034504 (2011).
[19] M. Asakawa, T. Hatsuda, and Y. Nakahara, Prog. Part. Nucl. Phys. **46**, 459 (2001).
[20] See, for example, the Appendix in Ref. [21].
[21] M. Kitazawa and F. Karsch, Nucl. Phys. **A830**, 223C (2009).
[22] F. Karsch and M. Kitazawa, Phys. Rev. D **80**, 056001 (2009).
[23] O. Kaczmarek, F. Karsch, M. Kitazawa, and W. Soldner, Phys. Rev. D **86**, 036006 (2012).
[24] G. Baym, J. P. Blaizot, and B. Svetitsky, Phys. Rev. D **46**, 4043 (1992).
[25] M. Kitazawa, T. Kunihiro, K. Mitsutani, and Y. Nemoto, Phys. Rev. D **77**, 045034 (2008).
[26] M. Le Bellac, *Thermal Field Theory* (Cambridge University Press, Cambridge, England, 1996).
[27] J. A. Mueller, C. S. Fischer, and D. Nickel, Eur. Phys. J. C **70**, 1037 (2010).
[28] J. S. Ball and T. W. Chiu, Phys. Rev. D **22**, 2542 (1980).
[29] M. Harada, M. Kurachi, and K. Yamawaki, Prog. Theor. Phys. **115**, 765 (2006).
[30] F. Gao, S. X. Qin, Y. X. Liu, C. D. Roberts, and S. M. Schmidt, Phys. Rev. D **89**, 076009 (2014).
[31] C. S. Fischer, J. Luecker, and C. A. Welzbacher, Phys. Rev. D **90**, 034022 (2014).
[32] T. Kim, M. Asakawa, and M. Kitazawa (to be published).
[33] C. Gale, Y. Hidaka, S. Jeon, S. Lin, J.-F. Paquet, R. D. Pisarski, D. Satow, V. V. Skokov, and G. Vujanovic, Phys. Rev. Lett. **114**, 072301 (2015).
[34] E. Braaten and R. D. Pisarski, Phys. Rev. D **46**, 1829 (1992).